Relationship between viscosity change and specificity in protein binding reaction studied by high-frequency wireless and electrodeless MEMS biosensor

Tomohiro Shagawa, Hiroomi Torii, Fumihito Kato, Hirotsugu Ogi*, and Masahiko Hirao

Graduate School of Engineering Science, Osaka University, Toyonaka, Osaka 560-8531, Japan

This study proposes a methodology for evaluating specific binding behavior between proteins using a resonance acoustic microbalance with a naked-embedded quartz (RAMNE-Q) biosensor. We simultaneously measured the frequency responses of fundamental (58 MHz) and 3rd-order (174 MHz) modes during multi step injections of proteins and deduced the thickness and viscosity evolutions of the protein layer. The viscosity increases with the progress of the binding reaction in nonspecific binding, but it markedly decreases in specific-binding cases. Thus, the high-frequency RAMNE-Q biosensor can be a powerful tool for evaluating specificity between proteins without measuring dissipation.

The evaluation of specific binding behavior is important for selectively detecting biomarkers, and it has remained a central issue in the diagnosis and life-science fields. The quartz crystal microbalance (QCM) biosensor is a mass-sensitive biosensor. It principally detects adsorbed mass on the quartz surface through a change in the resonance frequency,[1–4] and therefore achieves real-time monitoring of the binding behavior of biomolecules. Moreover, it is a label-free biosensor, which allows the intrinsic interactions of proteins to be evaluated. The QCM biosensor has been recently adopted for evaluation of the viscoelastic properties of protein layers, which are linked under binding conditions and in the structures of formed protein layers. This method requires dissipation measurement along with frequency measurement, which is known as the QCM-D technique.[5–7] However, the conventional QCM-D biosensors use thick quartz crystals with fundamental frequencies of 5-10 MHz, the resulting in reduced mass sensitivity. A low-frequency QCM also shows low sensitivity to the viscoelastic properties of thin protein layers: the acoustic shear field extends into the solution, and its decay length is inversely proportional to the square root of the frequency. For example, the decay length for a 5 MHz QCM reaches 250 nm from the quartz surface, which is much larger than the protein layer thickness in many assays, and little shear deformation occurs in such a thin layer with a low-frequency QCM, leading to the reduced sensitivity to the viscoelasticity in the protein layer due to the dominant contribution of the surrounding-liquid viscosity.

We previously developed a resonance acoustic microbalance with a naked-embedded quartz (RAMNE-Q), which is an electrodeless and wireless QCM fabricated by a MEMS process,[8,9]

*E-mail: ogi@me.es.osaka-u.ac.jp

where both surfaces and all sides of an electrodeless naked-quartz resonator can be used. The naked quartz crystal is supported without any fixed parts, and it is embedded in a microchannel fabricated in a Si wafer by sandwiching with two glass wafers. The electrodeless aspect of the RAMNE-Q biosensor makes it possible to perform a frequency measurement focusing on the viscoelasticity of the protein layer.

In this study, we propose a viscoelastic evaluation method using a high-frequency RAMNE-Q biosensor with a fundamental resonance frequency of 58 MHz. We simultaneously measured the fundamental-mode (58 MHz) and third-mode (174 MHz) frequency responses, and using a three-layer model[10–12] consisting of the quartz layer, the viscoelastic protein layer, and the viscous solution layer, we determined the evolutions of the protein layer thickness and viscosity only from the frequency changes without using dissipation. This is advantageous because dissipation is sensitive not only to a protein's viscoelasticity but also more significantly to many other factors, including changes in the solution viscosity, solution flow rate, holding condition of the resonator, and so forth. In particular, mechanical contacts to the resonator induce high ambiguity in the as-measured dissipation.[13] Thus, a viscoelasticity evaluation without dissipation measurement has been desired. To accomplish this, one needs to perform a QCM measurement at very high frequencies, to retain the high mass sensitivity, otherwise the frequency responses will not be separated. Although measurements of liquid viscosity using a 5 MHz QCM have been reported, where overtones of up to ∼200 MHz were used,[14,15] these methods have not been applied to protein layers. Previous QCM-D measurements of a thin protein layer were performed below 70 MHz. Therefore, the presence of electrodes may prevent high-sensitivity measurement of the viscoelasticity of protein layers at high frequencies. Thus, the high-frequency RAMNE-Q biosensor is ideal for the viscoelasticity measurement of a thin protein layer.

In the three-layer model, a Voigt viscoelastic layer is assumed for the protein layer, where a viscous damper and elastic spring are connected in parallel. Solving the wave equations with the boundary conditions of the stress free states at the bottom and top surfaces and assuming continuous of the shear stress and particle velocity with the non slip condition at each interface, the shift of the n th overtone resonance frequency from its free vibration Δf_n is given by

$$\Delta f_n \approx \mathrm{Im}\left(\frac{\beta}{2\pi\rho_q h_q}\right), \tag{1}$$

where

$$\begin{aligned} \beta &= \kappa_p\xi_p\frac{1-Ae^{2\xi_p h_p}}{1+Ae^{2\xi_p h_p}}, \\ A &= \frac{\kappa_p\xi_p+\kappa_s\xi_s\tanh(\xi_s h_s)}{\kappa_p\xi_p-\kappa_s\xi_s\tanh(\xi_s h_s)}, \end{aligned}$$

$$\begin{aligned}
\kappa_p &= \frac{\mu_p^*}{j\omega}, \kappa_s = \eta_s, \\
\xi_p &= \sqrt{-\frac{\rho_p\omega^2}{\mu_p^*}}, \xi_s = \sqrt{\frac{j\rho_s\omega}{\eta_s}}, \\
\mu_p^* &= \mu_p + j\omega\eta_p, \omega = 2\pi f_n, \\
f_n &= nf_1, f_1 = \frac{1}{2h_q}\sqrt{\frac{\mu_q}{\rho_q}}.
\end{aligned}$$

Here, h, ρ, μ, and η denote the thickness, mass density, shear modulus, and viscosity, respectively, and the subscripts q, p, and s represent the quantities in the quartz layer, protein layer, and solution layer, respectively. Because $\rho_q, \mu_q, \rho_s, and \eta_s$ are known properties, Eq. (1) is a function of h_p, η_p, μ_p, ρ_p, and n:

$$\Delta f_n = \Delta f_n(h_p, \eta_p, \mu_p, \rho_p, n). \tag{2}$$

We calculated shear-stress distributions in protein and solution layers using this model for quartz oscillators with $f_1 = 5$ and 58 MHz when the unit displacement amplitude is applied at the quartz surface (Fig. 1). A higher-frequency QCM causes much larger shear stress in the protein layer as well as less shear-field leakage into the solution layer. Thus, the advantages of a higher-frequency QCM are obvious.

We found that the contributions of μ_p and ρ_p to the resonance frequencies are considerably smaller than those of h_p and η_p, and we fixed them to be $\mu_p = 500$ kPa and $\rho_p = 1000$ kg/m^3, respectively, to reduce the ambiguity of the parameters in the analysis. (Changes in the fundamental resonance frequency caused by reasonable variations of μ_p and ρ_p are smaller than those caused by similar variations in h_p and η_p by factors of 50 and 5, respectively.) Thus, h_p and η_p are inversely determined using Eq. (1) with the two measured resonance frequencies.

Usual bioassays construct multiple protein layers, and the viscoelasticity of each layer is modified with every binding of a protein layer. The viscoelastic properties thus dynamically change during the formation of multiple protein layers, and evaluation of the viscoelasticity of individual layers is complicated and unrealistic. We thus evaluate the macroscopic viscoelasticity of multiple protein layers by regarding them as a single layer. Even with this simple assumption, we clearly observe a difference in the viscosity between specific and nonspecific binding as follows.

The RAMNE-Q biosensor with a 58 MHz quartz resonator was washed by a piranha solution (98% H_2SO_4: 33% H_2O_2 =7:3) for 30 min, rinsed with ultrapure water, and cleaned by a UV-ozone cleaner. It was then installed in the sensor cell. The two flat antennas set outside the microchannel generated and detected the shear vibration of the quartz wirelessly during the solution flow. We used a phosphate-buffered saline (PBS) solution as the running buffer. The electrodeless measurement is affected by the ionization degree of the solution. The

resonance-peak amplitude, for example, decreases as the NaCl concentration in the solution increases: It becomes one-fifth of the original value upon the addition of 1 M NaCl.[9] However, the PBS solution used in this study contains less than 0.05 M NaCl, leading to insignificant changes in the amplitude and dissipation. Furthermore, such an ionization effect is involved in the baselines, and its influence on the viscoelasticity evaluation will be negligible because the changes in frequency from the baselines are used. To investigate the difference in the viscosity of the protein layer between specific and nonspecific bindings, we performed a multistep injection as follows. First, streptococcal protein G (SPG) solution (200 μg/ml in PBS) was injected to immobilize SPG molecules directly (nonspecifically) on the quartz surfaces, and the surfaces were rinsed with the buffer solution (PBS solution). Bovine serum albumin (BSA) solution (1 mg/ml in PBS) was then injected to immobilize BSA molecules nonspecifically on the quartz surfaces to block uncovered quartz areas. After that, anti-C-reactive-protein (anti-CRP) antibody solution (200 μg/ml in PBS) was injected to construct an oriented receptor layer through the specific binding between SPG molecule and the Fc region of anti-CRP-antibody molecules. After rinsing with the buffer solution, CRP solution (10 ng/ml in PBS) was injected to detect the specific binding reaction between the oriented anti-CRP-antibody and CRP molecules. The quartz surfaces were rinsed with the buffer solution, and finally, a 100 ng/ml CRP solution was injected.

Figure 2 shows the measured frequency responses of each injection, indicating the successful detection of injected molecules even for a low-concentration analyte (10 ng/ml). It is revealed that a significant difference appears in the frequency response between the nonspecific and specific bindings. In the specific-binding cases (anti-CRP-antibody and 10 ng/ml CRP injections), the two frequencies are clearly separated, while they show similar changes in the nonspecific-binding cases (SPG and BSA injections). The frequencies were not separated for the last injection of 100 ng/ml CRP despite the specific binding. Because the binding sites of anti-CRP antibody were occupied by the previous injection, the injection of 100 ng/ml CRP caused nearly nonspecific binding rather than specific binding.

Such a difference between specific- and nonspecific-binding behaviors is explicitly demonstrated in Fig. 3, where the evolutions of the total thickness and the macroscopic viscosity of the protein layer are shown. The total thickness increases during each injection, while the viscosity significantly decreases in the case of specific bindings. The injections of SPG and BSA formed a protein layer with higher viscosity ($>\sim$2 mPa·s), indicating higher energy loss due to the viscoelastic movement of the protein layer responding to the quartz surface [Fig. 4(a)]. The most important observation here is that injections of anti-CRP antibody and CRP markedly decrease the viscosity of the overall protein layer. This indicates that the specific bindings between SPG and anti-CRP antibody and between anti-CRP antibody and CRP construct a truss-like molecule network, producing a rigid-layer structure as illustrated in

Fig. 4(b), which allows the protein layer to follow the quartz-surface movement. Thus, the decrease in the macroscopic viscosity, corresponding to a reduced energy loss in the protein layer, represents the construction of a stable and robust protein layer. The final injection of the higher-concentration CRP caused a slight increase in the viscosity, implying the formation of a lossy region at the top of the protein layer [Fig. 4(c)]. Such a strong correlation between the viscosity and the specificity of binding has never been reported and can only be observed with a high-frequency electrodeless QCM.

Using a RAMNE-Q biosensor with a fundamental resonance frequency of 58 MHz, we deduced the evolutions of the thickness and viscosity of protein layers without measuring dissipation. We found significant difference in the viscosity of the formed protein layer in specific and nonspecific bindings. Nonspecific binding forms a viscous (lossy) protein layer but subsequent specific bindings make the overall protein layer much more robust. Thus, this method will be a powerful tool for evaluating the specificity among protein interactions.

Acknowledgement

This study was supported by the Funding Program for Next Generation World-Leading Researchers by the Cabinet Office, Government of Japan.

References

1) G. Sauerbrey, Z. Phys. **155**, 206 (1959) [in German].
2) H. Muramatsu, M. Dicks, E. Tamiya, and I. Karube, Anal. Chem. **59**, 2760 (1987).
3) Y. Liu, X. Yu, R. Zhao, D. Shangguan, Z. Bo, and G. Liu, Biosens. Bioelectron. **19**, 9 (2003).
4) H. Ogi, H. Nagai, Y. Fukunishi, T. Yanagida, M. Hirao, and M. Nishiyama, Jpn. J. Appl. Phys. **49**, 07HD07 (2010).
5) F. Höök, B. Kasemo, T. Nylander, C. Fant, K. Sott, and H. Elwing, Anal. Chem. **73**, 5796 (2001).
6) A. Patel, K. Kanazawa, and C. W. Frank, Anal. Chem. **81**, 6021 (2009).
7) M. Yan, C. Liu, D. Wang, J. Ni, and J. Chang, Langmuir **27**, 9860 (2011).
8) F. Kato, H. Ogi, T. Yanagida, S. Nishikawa, M. Nishiyama, and M. Hirao, Jpn. J. Appl. Phys. **50**, 07HD03 (2011).
9) F. Kato, H. Ogi, T. Yanagida, S. Nishikawa, M. Hirao, and M. Nishiyama, Biosens. Bioelectron. **33**, 139 (2012).
10) C. Reed, K. Kanazawa, and J. H. Kaufman, J. Appl. Phys. **68**, 1993 (1990).
11) M. V. Voinova, M. Jonson, and B. Kasemo, J. Phys. Condens. Matter. **9**, 7799 (1997).
12) M. V. Voinova, M. Rodahl, M. Jonson, and B. Kasemo, Phys. Scri. **59**, 391 (1999).
13) H. Ogi, M. Hirao, and T. Honda, J. Acoust. Soc. Am. **98**, 458 (1995).
14) T. Yamaguchi, M. Hayakawa, T. Matsuoka, and S. Koda, J. Phys. Chem. B **113**, 11988 (2009).
15) T. Yamaguchi, K. Mikawa, and S. Koda, Bull. Chem. Soc. Jpn. **85**, 6 701 (2012).

Figure Captions

Fig. 1. (Color online) Shear-stress distributions on quartz oscillators with fundamental resonance frequencies of 5 and 58 MHz. The dashed vertical line indicates the interface between the protein and solution layers. The parameters used are as follows: $h_s = 1000$ nm, $\rho_s = 1000$ kg/m^3, $\eta_s = 0.001$ Pa·s, $h_p = 20$ nm, $\rho_p = 1000$ kg/m^3, $\eta_p = 0.002$ Pa·s, $\mu_p = 500$ kPa.

Fig. 2. (Color online) Frequency responses during the multi-injection procedure. Black and red lines are measurements of the fundamental (58 MHz) and 3rd (174 MHz) modes, respectively. The same vertical range is used for all figures.

Fig. 3. (Color online) Evolutions of the total thickness (upper) and viscosity (lower) of the protein layer calculated with the three layer model. Black, red, blue, green, and yellow lines are obtained from measurements of (a), (b), (c), (d), and (e) in Fig. 2, respectively.

Fig. 4. (Color online) Schematics of possible protein structures on the quartz surface. (a) Nonspecifically adsorbed SPG and BSA molecules cause viscoelastic deformation in response to the quartz-surface movement, leading to higher viscosity. (b) Construction of protein network to form a stable and rigid layer. (c) Further loading of the CRP molecules causes nonspecific binding because of previously occupied binding sites, leading to an increase in the viscosity.

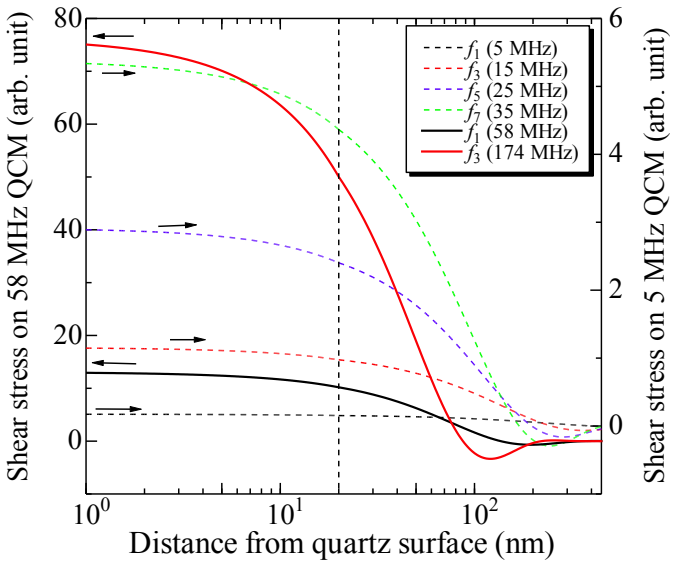
Shear stress on 58 MHz QCM (arb. unit)
Shear stress on 5 MHz QCM (arb. unit)
Distance from quartz surface (nm)
f_1 (5 MHz)
f_3 (15 MHz)
f_5 (25 MHz)
f_7 (35 MHz)
f_1 (58 MHz)
f_3 (174 MHz)
80
60
40
20
0
6
4
2
0
10^0
10^1
10^2

Fig. 1.

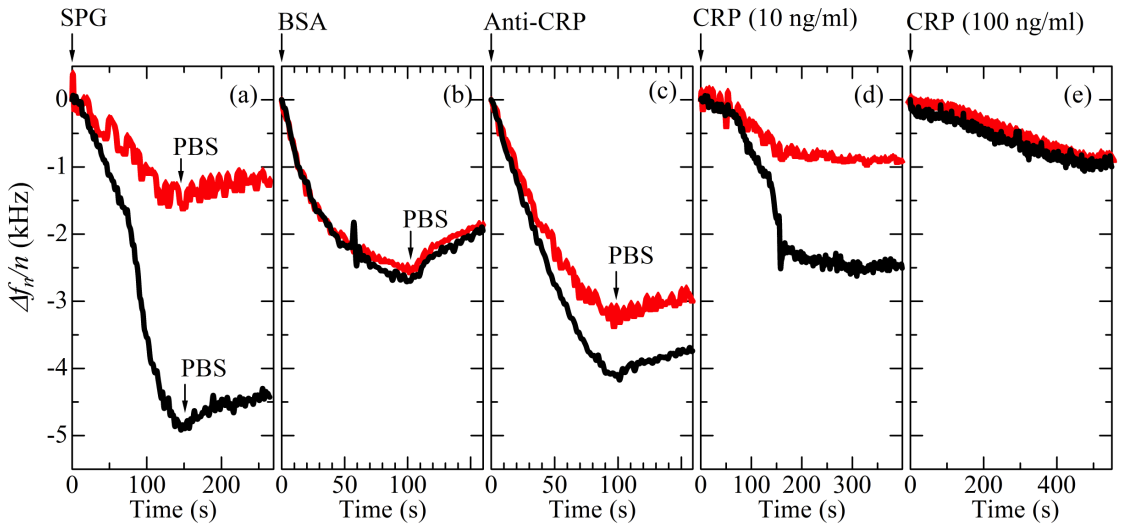
SPG
BSA
Anti-CRP
CRP (10 ng/ml)
CRP (100 ng/ml)
(a)
(b)
(c)
(d)
(e)
PBS
PBS
PBS
PBS
$\Delta f_n/n$ (kHz)
0
-1
-2
-3
-4
-5
0 100 200
0 50 100
0 50 100
0 100 200 300
0 200 400
Time (s)
Time (s)
Time (s)
Time (s)
Time (s)

Fig. 2.

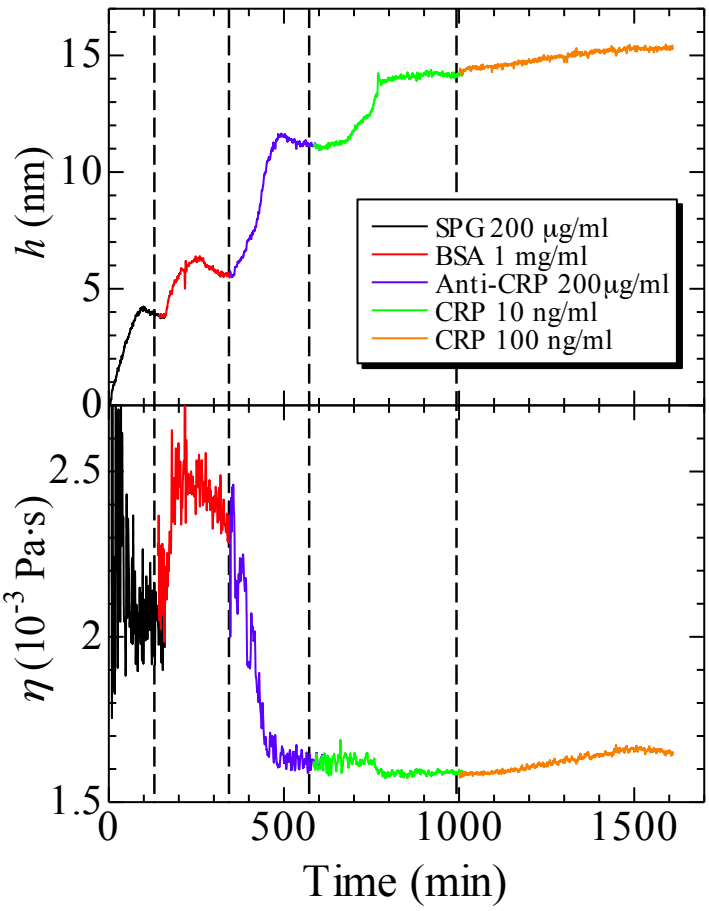
15
10
5
0
h (nm)
SPG 200 μg/ml
BSA 1 mg/ml
Anti-CRP 200μg/ml
CRP 10 ng/ml
CRP 100 ng/ml
2.5
2
1.5
η (10-3 Pa·s)
0
500
1000
1500
Time (min)

Fig. 3.

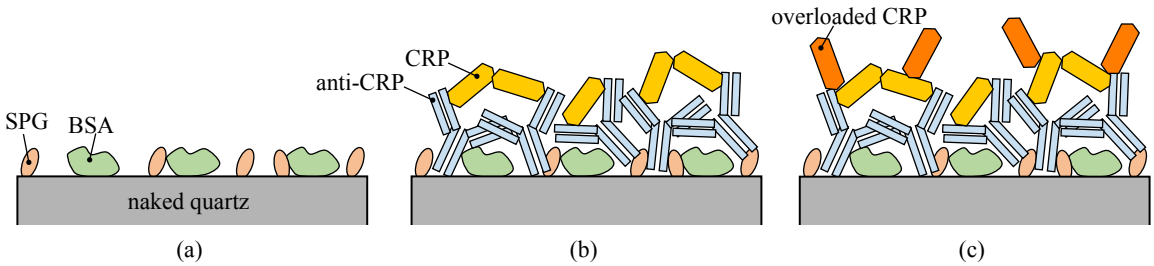

Fig. 4.